JACC: CARDIOVASCULAR INTERVENTIONS VOL. 7, NO. 7, 2014

ISSN 1936-8798/$36.00
PUBLISHED BY ELSEVIER INC. http://dx.doi.org/10.1016/j.jcin.2014.03.004

Fractional Flow Reserve Calculation From 3-Dimensional Quantitative Coronary Angiography and TIMI Frame Count

A Fast Computer Model to Quantify the Functional Significance of Moderately Obstructed Coronary Arteries

Shengxian Tu, PhD,* Emanuele Barbato, MD, PhD,† Zsolt Köszegi, MD, PhD,‡ Junqing Yang, MD,§ Zhonghua Sun, MD,‖ Niels R. Holm, MD,¶ Balázs Tar, MD,‡ Yingguang Li, MSc,* Dan Rusinaru, MD,† William Wijns, MD, PhD,† Johan H.C. Reiber, PhD*

Leiden, the Netherlands; Aalst, Belgium; Nyiregyyhaza, Hungary; Guangzhou and Tianjin, China; and Skejby, Denmark

Objectives This study sought to present a novel computer model for fast computation of myocardial fractional flow reserve (FFR) and to evaluate it in patients with intermediate coronary stenoses.

Background FFR is an indispensable tool to identify individual coronary stenoses causing ischemia. Calculation of FFR from x-ray angiographic data may increase the utility of FFR assessment.

Methods Consecutive patients with intermediate coronary stenoses undergoing pressure wire-based FFR measurements were analyzed by a core laboratory. Three-dimensional quantitative coronary angiography (QCA) was performed and the mean volumetric flow rate at hyperemia was calculated using TIMI (Thrombolysis In Myocardial Infarction) frame count combined with 3-dimensional QCA. Computational fluid dynamics was applied subsequently with a novel strategy for the computation of FFR. Diagnostic performance of the computed FFR (FFR_{QCA}) was assessed using wire-based FFR as reference standard.

Results Computation of FFR_{QCA} was performed on 77 vessels in 68 patients. Average diameter stenosis was 46.6 ± 7.3%. FFR_{QCA} correlated well with FFR ($r = 0.81$, $p < 0.001$), with a mean difference of 0.00 ± 0.06 ($p = 0.541$). Applying the FFR cutoff value of ≤0.8 to FFR_{QCA} resulted in 18 true positives, 50 true negatives, 4 false positives, and 5 false negatives. The area under the receiver-operating characteristic curve was 0.93 for FFR_{QCA}, 0.73 for minimum lumen area, and 0.65 for percent diameter stenosis.

Conclusions Computation of FFR_{QCA} is a novel method that allows the assessment of the functional significance of intermediate stenosis. It may emerge as a safe, efficient, and cost-reducing tool for evaluation of coronary stenosis severity during diagnostic angiography. (J Am Coll Cardiol Intv 2014;7:768–77) © 2014 by the American College of Cardiology Foundation

From the *Division of Image Processing, Department of Radiology, Leiden University Medical Center, Leiden, the Netherlands; †Cardiovascular Center Aalst, Onze-Lieve-Vrouwziekenhuis (OLV) Hospital, Aalst, Belgium; ‡Invasive Cardiology Laboratory, Jósa András Teaching Hospital, Nyíregyháza, Hungary; §Department of Cardiology, Guangdong General Hospital, Guangzhou, China; ‖Department of Cardiology, TEDA International Cardiovascular Hospital, Tianjin, China; and the ¶Department of Cardiology, Aarhus University Hospital, Skejby, Denmark. Dr. Tu and Mr. Li are employed by Medis and have research appointments at the Leiden University Medical Center (LUMC). Drs. Barbato and Wijns have received institutional grant support and consultancy fees paid to Cardiovascular Research Center Aalst from St. Jude Medical and other device and pharmaceutical companies. Dr. Holm has received speaker fees, consulting fees, and research grants from St. Jude Medical; research grants and consulting fees from Terumo; consulting fees from Acarix; and a research grant from Medtronic. Dr. Reiber is the chief executive officer of Medis and has a part-time appointment at LUMC as a professor of medical imaging. All other authors have reported that they have no relationships relevant to the contents of this paper to disclose.

Manuscript received February 28, 2014; revised manuscript received March 21, 2014, accepted March 27, 2014.

Accurate assessment of stenosis severity by coronary angiography is essential for physicians in clinical decision making regarding the need for myocardial revascularization. Equally important is the functional significance of coronary stenoses, both for its symptomatic and prognostic consequences (1). The anatomical details imaged by coronary angiography do not completely reflect the entire physiological impact on the circulation, and hence, it frequently fails to identify the accurate hemodynamic significance of the stenosis, particularly in the category of intermediate stenosis (2,3). Pressure-derived fractional flow reserve (FFR) is a precise index revealing the ischemic potential of individual lesions. Several clinical trials have documented that the combined angiography-FFR evaluation and FFR-guided coronary intervention were associated with favorable clinical outcome, while reducing unnecessary revascularization (1,2).

See page 778

Despite the potential clinical and economic benefits, the adoption of FFR has been slow in many countries. A tool that could accurately and rapidly calculate FFR without the need of a costly pressure wire would make this physiologic index become available to a wider population. Computational fluid dynamics (CFD) has been applied to coronary computed tomography angiography for the computation of FFR (FFR_{CT}). However, the accuracy of FFR_{CT} was mixed in 2 prospective studies (4,5) and the diagnostic accuracy of the current FFR_{CT} algorithm remains suboptimal (6). A more recent study applied CFD to rotational angiography for the computation of virtual FFR (7). High accuracy was reported, but the interrogated lesions were simple lesions. In addition, it required up to 24 h for the computation, making this approach less attractive.

The objective of this study was to present a new approach on the basis of 3-dimensional (3D) quantitative coronary angiography (QCA) and TIMI (Thrombolysis In Myocardial Infarction) frame count for fast computation of FFR in patients with coronary artery disease. The accuracy of the computed fractional flow reserve (FFR_{QCA}) was evaluated in patients with intermediate coronary stenoses using pressure wire-based FFR as reference standard.

Methods

Study design. This was an observational and analytical study. Patients who had undergone coronary angiography and FFR assessment with recorded hyperemic projections in the context of approved trial or routine clinical evaluation when frame count–based coronary flow reserve (CFR) was evaluated could be included. Three hospitals (Jósa András Teaching Hospital, Nyíregyháza, Hungary; Guangdong General Hospital, Guangzhou, China; and TEDA International Cardiovascular Hospital, Tianjin, China) provided retrospective data for the post-hoc analysis. After complete data analysis, another hospital (OLV Hospital, Aalst, Belgium) that uses FFR guidance in daily practice (8) acquired prospective data to be used as an independent testing group. The study was approved by the local ethics committees at the participating hospitals, and patients provided written informed consent. Imaging data were analyzed at a core laboratory (ClinFact, Leiden, the Netherlands).

Study population. For the post-hoc analysis, consecutive patients who underwent diagnostic angiography between October 1, 2011 and June 15, 2013 with documented FFR fulfilling the following criteria were included: 1) FFR was interrogated on de novo intermediate lesions (40% to 70% diameter stenosis by visual estimation) of the major epicardial coronary arteries; 2) no coronary artery bypass graft had been implanted to supply the interrogated vessel; 3) no ostial left main stenosis was identified when screening the diagnostic angiography; 4) 2 angiographic projections $\geq 25^{\circ}$ apart were recorded by flat-panel systems; 5) nitroglycerine was given prior to angiographic acquisitions; and 6) at least 1 angiographic projection was recorded during hyperemia. Patients were excluded for any of the following reasons: 1) the interrogated vessel had too much overlap or foreshortening (>90%); 2) the image quality of the hyperemic projection was not sufficient to evaluate by frame count; and 3) the mean pressure of the guiding catheter or blood hematocrit value was not documented. The group of prospectively enrolled patients was included in a single center from July 1, 2013 to August 1, 2013, applying the same inclusion and exclusion criteria.

Abbreviations and Acronyms

3D = 3-dimensional
CFD = computational fluid dynamics
CFR = coronary flow reserve
CI = confidence interval
DS% = percent diameter stenosis
FFR = fractional flow reserve
FFR_{CT} = computation of fractional flow reserve using coronary computed tomography angiography
IQR = interquartile range
MLA = minimum lumen area
QCA = quantitative coronary angiography
TIMI = Thrombolysis In Myocardial Infarction
VFR = volumetric flow rate

Strategy for the computation of FFR_{QCA}. Computation of FFR by CFD requires methods to extract anatomical models from imaging data and to incorporate hemodynamic boundary conditions. Our strategy was to reconstruct anatomical models by 3D QCA and apply CFD subsequently, using the hyperemic flow rate derived by 3D QCA and TIMI frame count at the boundaries. When bifurcations were reconstructed, the reference, that is, the computer-reconstructed normal lumen as if the lesion was not present, was used to determine the flow distribution from the mother vessel into the 2 daughter branches.

Three-dimensional QCA. Angiographic images were recorded at 30 frames/s (59.7% of cases) or 15 frames/s by monoplane or biplane x-ray systems (AXIOM-Artis,

Siemens, Malvern, Pennsylvania; Innova, GE Healthcare, Chalfont, Buckinhamshire, United Kingdom; AlluraXper, Philips Heathcare, Best, the Netherlands; INTEGRIS, Allura, Philips). An experienced analyst blinded to the wire-based FFR values used a validated software (QAngio XA 3D research edition 1.0, Medis Special BV, Leiden, the Netherlands) (9) to perform 3D QCA. The angiographic reconstruction was previously described (9). Side branches with diameters larger than one-third of the main vessel diameter and without significant overlap were included in 3D reconstruction. The bifurcation diameter models (10) that described the physical relations of the normal mother vessel with regard to the daughter branches were used to optimize the reference vessel diameters. Multiple bifurcations in the same interrogated vessel were merged into tree structure if applicable.

Minimum lumen diameter, reference vessel diameter, minimum lumen area (MLA), percent diameter stenosis (DS%), percent area stenosis, intraluminal plaque volume, lesion eccentricity index, and bifurcation angle if applicable were available. The intraluminal plaque volume was defined as the space between the reference vessel and the lumen.

Volumetric flow rate. The contrast medium transport time in the reconstructed vessel was calculated on hyperemic projections using TIMI frame count, blinded to the FFR values. Figures 1E1 to 1E9 show consecutive image frames at hyperemia. When multiple hyperemic projections were available, the shortest transport time was used. The mean volumetric flow rate (VFR) at hyperemia was derived using the lumen volume of the reconstructed coronary tree divided by the mean transport time.

The same calculation was applied to the baseline angiography, from which the baseline VFR was obtained. CFR was derived by dividing the hyperemic VFR by the baseline VFR.

Computational fluid dynamics. The reconstructed geometries were discretized using ICEM (version 14.0, ANSYS Inc., Canonsburg, Pennsylvania) with tetrahedral cells (meshing). The Navier-Stokes equations were implemented in each cell and nonlinear partial differential equations were solved simultaneously using FLUENT (version 14.0, ANSYS Inc.). Blood was modeled as incompressible Newtonian fluid. The blood density and viscosity were derived using the hematocrit value of individual patients. The mean hyperemic VFR and the mean pressure at the guiding catheter tip were applied at the inlet, whereas outflow (fully developed flow) condition was applied at the outlets. Finite volume method with element size between 0.02 mm and 0.2 mm automatically adapted to the complexity of the local anatomy and parallel computing were used. After simulation, FFR_{QCA} was defined as the mean pressure at the outlet divided by the mean pressure at the inlet. When bifurcations were included, flow distribution from the mother vessel into the 2 daughter branches needed to be specified in this approach. We used the RVD and bifurcation angles to automatically determine the flow distribution at the bifurcation; more blood will flow into the daughter branch having larger RVD and larger take-off angle with the mother (proximal main) branch.

Reproducibility in computer modeling. To test the reproducibility in computing FFR_{QCA} from the same angiographic data, all analytical steps were repeated on 10 randomly selected vessels by the same analyst 2 weeks later and by another analyst, blinded to each result. The intraobserver and interobserver variability was reported.

Measurement of wire-based FFR and validation. FFR was measured in all cases using the RadiAnalyzer Xpress instrument (St. Jude Medical, Uppsala, Sweden) and a coronary pressure wire (Certus, St. Jude Medical). After calibration and equalization, the pressure wire was advanced distally to the stenosis until the pressure sensor landed in a smooth coronary segment. Hyperemia was induced by administration of adenosine or adenosine 5′-triphosphate, at least 100 μg by intracoronary administration or 140 μg/kg/min by intravenous administration. The pressure sensor was returned to the guiding catheter tip to exclude pressure drift.

For the retrospective data, the computed FFR_{QCA} was compared with the matched FFR at the core laboratory. For the prospective data, the same comparison was performed by an independent cardiologist at the hospital.

Statistical analysis. Continuous variables are expressed as mean ± SD if normally distributed or as median (interquartile range [IQR]) if non-normally distributed. Categorical variables are expressed as percentages. Data were analyzed on a per-patient basis for the clinical characteristics and on a per-vessel basis for the remaining calculations. Pearson correlation was used to quantify the correlation between FFR and FFR_{QCA}, whereas Spearman correlation was used to quantify the correlations between FFR and 3D QCA. Agreement between FFR and FFR_{QCA} was assessed by Bland-Altman plot. The performance of FFR_{QCA} in predicting functionally significant stenosis was assessed using sensitivity, specificity, positive predictive value, negative predictive value, and diagnostic accuracy, together with their 95% confidence intervals (CIs). The area under the curve by receiver-operating characteristic analysis was used to assess the diagnostic accuracy of FFR_{QCA} and 3D QCA. The Youden index was used as criterion to identify the best cutoff value for MLA in predicting functionally significant stenosis, whereas the commonly used value (50%), was used for DS%. Paired comparisons between receiver-operating characteristic curves were performed by the DeLong method using MedCalc (version 13.0, MedCalc Software BVBA, Ostend, Belgium). Other statistical analyses were performed with IBM SPSS (version 20.0, Armonk, New York). Continuous variables were compared with Student *t* test. A 2-sided value of <0.05 was considered to be significant.

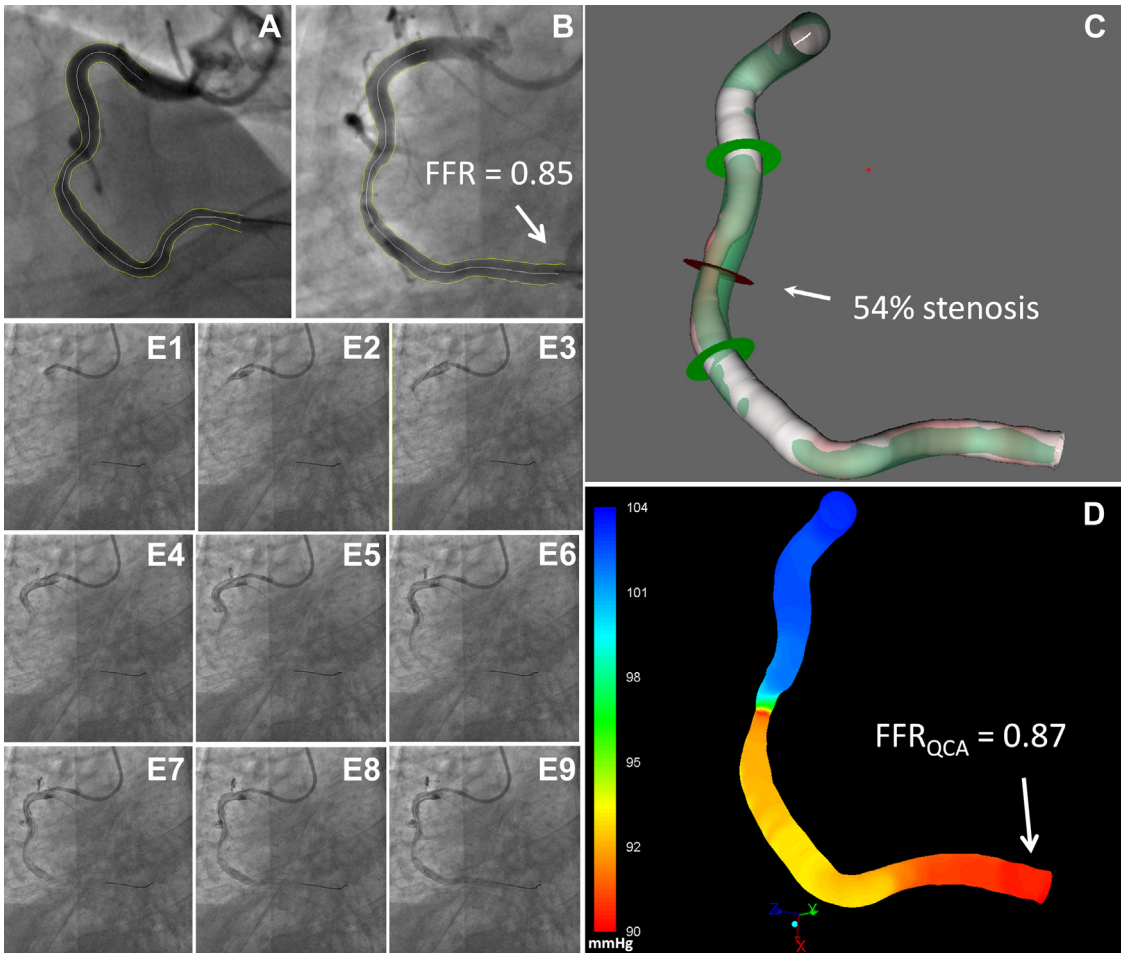

Figure 1. Computation of FFR From 3D QCA and TIMI Frame Count

(A,B) X-ray angiography showing the interrogated lesion with superimposed lumen contours. In **(B)** the **arrow** points to the location where the FFR was measured by pressure wire. **(C)** Three-dimensional (3D) angiographic reconstruction of arterial lumen and reference vessel. The **arrow** points to the location with the maximum diameter stenosis (54%). **(D)** Simulated pressure distribution at hyperemia: The computed quantitative coronary artery (QCA) fractional flow reserve (FFR [FFR_{QCA}]) was 0.87, whereas the wire-based FFR was 0.85. The **arrow** points to the location where the FFR_{QCA} was reported. **(E1 to E9)** Consecutive angiographic image frames at hyperemia. TIMI = Thrombolysis In Myocardial Infarction.

Results

Baseline clinical and lesion characteristics. A total of 80 vessels with intermediate stenosis from 71 patients were included. Three patients were excluded on the basis of the aforementioned exclusion criteria, resulting in 77 vessels (49 left anterior descending arteries, 13 left circumflex arteries, 13 right coronary arteries, 2 diagonal arteries) in 68 patients for analysis. The independent testing group included 22 vessels in 20 patients. The clinical characteristics are listed in Table 1. Intracoronary administration of vasodilators was used in 33 vessels (42.9%) for FFR measurement and intravenous administration was applied in the remaining 44 vessels (57.1%). Table 2 shows the lesion characteristics. Lesions involved coronary bifurcations in 46 cases (59.7%). The interrogated vessels had an average DS%, minimum lumen diameter, and FFR of 46.6 ± 7.3%, 1.51 ± 0.35 mm, and 0.82 ± 0.11 mm (median: 0.84 [IQR: 0.78 to 0.89 mm]), respectively. Abnormal FFR ≤0.8 was measured in 23 vessels (29.9%).

Correlation and agreement between FFR and FFR_{QCA}. The mean pressure at the guiding catheter tip was 86 ± 14 mm Hg at hyperemia. Representative examples of computation of FFR_{QCA} are shown in Figures 1 and 2. FFR_{QCA} had an average value of 0.82 ± 0.10 (median: 0.83 [IQR: 0.77 to 0.88]). Figure 3 shows agreement between FFR_{QCA} and wire-based FFR. Good correlation ($r = 0.81$; $p < 0.001$) and agreement (mean difference:

Table 1. Baseline Clinical Characteristics (n = 68)

Age, yrs	62.0 ± 9.0
Male	47 (69.1)
Mean body mass index, kg/m^2	27.5 (24.8–30.8)
Hypertension	47 (69.1)
Hyperlipidemia	52 (76.5)
Current smoker	16 (23.5)
Diabetes mellitus	20 (29.4)
Angina type	
Stable angina	52 (76.5)
Unstable angina	9 (13.2)
Silent ischemia	6 (8.8)
Cardiovascular history	
Previous myocardial infarction	15 (22.1)
Previous PCI	22 (32.4)
Previous CABG	3 (4.4)

Values are mean ± SD, n (%), or median (IQR).
CABG = coronary artery bypass graft; IQR = interquartile range; PCI = percutaneous coronary intervention.

Table 2. Baseline Lesion Characteristics (n = 77)

Index artery	
Left anterior descending artery	49 (63.6)
Left circumflex artery	13 (16.9)
Right coronary artery	13 (16.9)
Diagonal artery	2 (2.6)
Bifurcation lesions	50 (64.9)
Fractional flow reserve	
Mean ± SD	0.82 ± 0.11
Median (IQR)	0.84 (0.78–0.89)
Percent diameter stenosis	46.6 ± 7.3
Percent area stenosis	64.6 ± 9.6
Minimum lumen diameter, mm	1.51 ± 0.35
Reference vessel diameter, mm	2.82 ± 0.52
Minimum lumen area, mm^2	2.06 (1.49–2.51)
Intraluminal plaque volume, mm^3	67.8 (41.7–81.9)
Lesion eccentricity index	0.24 (0.16–0.31)

Values are n (%), mean ± SD, or median (IQR). Anatomical parameters were quantified by 3-dimensional quantitative coronary angiography.
IQR = interquartile range.

0.00 ± 0.06; p = 0.541) between FFR_{QCA} and FFR were found.

DS% was not significantly different between the retrospective and prospective groups (47.3 ± 7.35 vs. 44.6 ± 7.05; p = 0.494). The deviation of FFR_{QCA} with respect to FFR between these 2 groups was not statistically significant (0.01 ± 0.05 vs. −0.01 ± 0.07; p = 0.291). The results were not significantly affected by administration route of vasodilators with deviation of intracoronary versus intravenous administration being 0.01 ± 0.05 vs. −0.00 ± 0.06 (p = 0.184), nor by the angiographic frame rate of 15 frames/s versus 30 frames/s (−0.01 ± 0.06 vs. 0.01 ± 0.06; p = 0.229).

Accuracy of FFR_{QCA} for diagnosis of functionally significant stenoses. Using the commonly used FFR cutoff value of ≤0.80, FFR_{QCA} had a higher area under the curve (0.93 [95% CI: 0.86 to 0.99]) than did MLA (0.73 [95% CI: 0.61 to 0.85]; difference: 0.20 [95% CI: 0.06 to 0.33]; p < 0.01) and DS (0.65 [95% CI: 0.51 to 0.79]; difference: 0.28 [95% CI: 0.14 to 0.42]; p < 0.01) quantified by 3D QCA (Fig. 4). Applying the discrimination limit of FFR_{QCA} ≤0.80 to 77 coronary vessels with intermediate stenosis resulted in 18 true positives, 50 true negatives, 4 false positives, and 5 false negatives. The diagnostic performance of FFR_{QCA} versus MLA and DS% is listed in Table 3. The best cutoff value for MLA in determining FFR ≤0.80 was found at 2.11 mm^2. FFR_{QCA} substantially improved the diagnostic performance of coronary angiography, with overall accuracy, sensitivity, specificity, positive predictive value, and negative predictive value of 88%, 78%, 93%, 82%, and 91%, respectively.

Volumetric flow rate and coronary flow reserve. The computed VFR was 1.18 ml/s (IQR: 0.86 to 1.49 ml/s) at baseline and 2.37 ml/s (IQR: 1.88 to 3.15 ml/s) at hyperemia. Scatterplot of CFR with respect to baseline VFR is presented in Figure 5. CFR tended to decrease with increasing baseline VFR (CFR = −0.54 × baseline VFR + 2.97, r = −0.38; p = 0.001). Wide scatter was observed, especially in vessels with low baseline VFR.

Correlation between FFR and anatomical indices. Table 4 shows the correlations between the measured FFR and 3D QCA. Poor to modest correlations were found and MLA had the highest correlation with FFR (r = 0.40, p < 0.001). The correlation between FFR and DS% was weak (r = -0.26, p = 0.025). Scatterplots are presented in Figure 6.

Computational performance of FFR_{QCA}. The 3D QCA took approximately 1 min per bifurcation reconstruction including the time required by user interaction. The same meshing scheme was applied to all cases, resulting in an average of 778,000 ± 456,000 cells per case. Approximately 1 min was required to generate the interior meshes after 3D reconstruction and 5 min for the CFD simulation on a workstation with a quad-core Intel Xeon E3-1225 processor (Intel Corporation, Santa Clara, California) (3.20 GHz) and 8 GB of RAM. The entire analysis typically took <10 min.

Reproducibility in modeling FFR_{QCA}. The analytical variability in computing FFR_{QCA} is presented in Table 5. The sum of all sources of variability contributed to an intraobserver variability of 0.00 ± 0.03 and an interobserver variability of 0.01 ± 0.03 in modeling FFR_{QCA} from the same angiographic data.

Discussion

We have developed a new computer model for fast computation of FFR from angiographic images alone. When applying the model in coronary vessels with

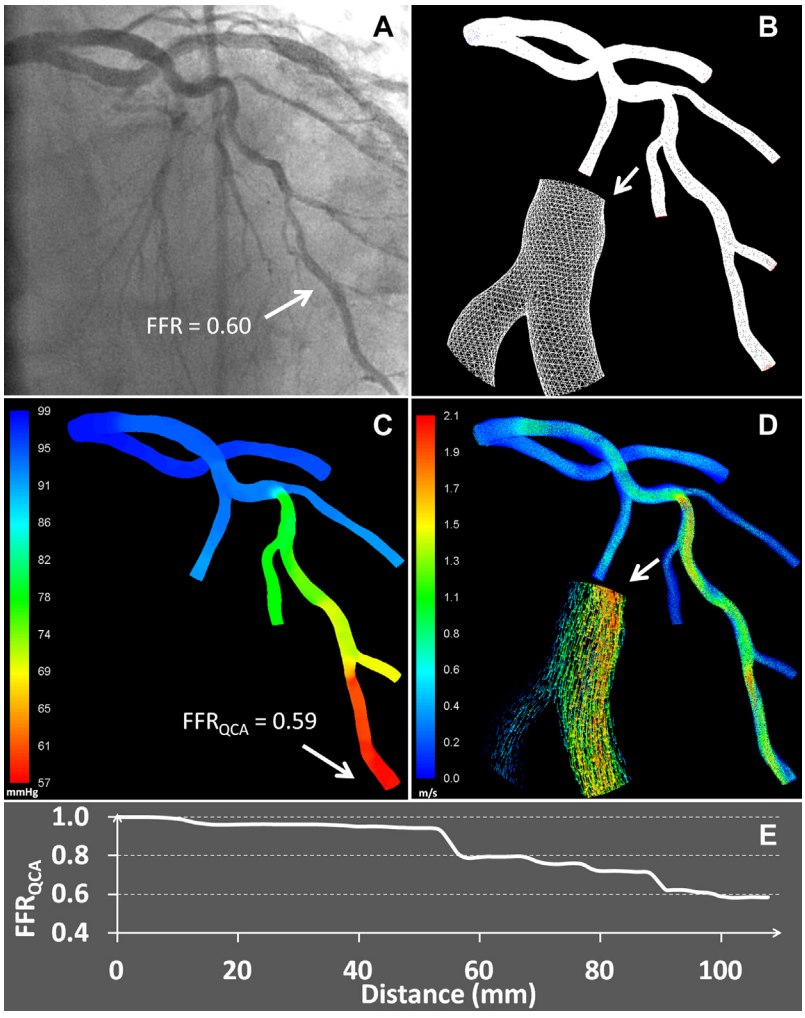

Figure 2. Angiographic Reconstruction of the Left Coronary Tree and Computation of FFR

(A) X-ray angiography showing diffused stenoses at the left anterior descending artery. **(B)** Three-dimensional angiographic reconstruction and the generated meshes. **(C)** Simulated pressure distribution at hyperemia. The computed FFR_{QCA} was 0.59 and the wire-based FFR was 0.60 at the distal position indicated by the **arrow**. **(D)** Simulated hyperemic flow colored by the velocity magnitude. **(E)** Virtual "reversed" FFR pullback along the centerline of the left anterior descending artery. Abbreviations as in Figure 1.

intermediate stenosis, the computed physiological index, that is, FFR_{QCA}, showed good correlation ($r = 0.81$, $p < 0.001$) and agreement (mean difference: 0.00 ± 0.06, $p = 0.541$) with the wire-based FFR. The overall accuracy of FFR_{QCA} for the diagnosis of ischemia defined by FFR $\leq$0.80 was 88%, with positive and negative predictive values of 82% and 91%, respectively.

The level of accuracy and precision was achieved in a challenging population of only intermediate stenoses with average diameter stenosis of $46.6 \pm 7.3\%$ and involving bifurcation in as many as 64.9% of cases. In such population, the accuracy of MLA and DS% was 64% and 68% for the diagnosis of ischemia defined by FFR $\leq$0.80. The improvement in the diagnostic accuracy by FFR_{QCA} as compared to 3D QCA was contributed by coupling flow and various anatomical details in the framework of CFD. It integrated accurate vessel dimensions from 3D QCA and individual hyperemic flow in solving the well-established Navier-Stokes equations, resulting in an accurate calculation of FFR.

Online capability. Instead of using generic boundary conditions, we applied "fixed" boundary conditions that led to a fast simulation approach. The simulation took approximately 5 min for each case. It is likely that advancements in computers will significantly reduce this computational time, resulting in a practical online approach. Although

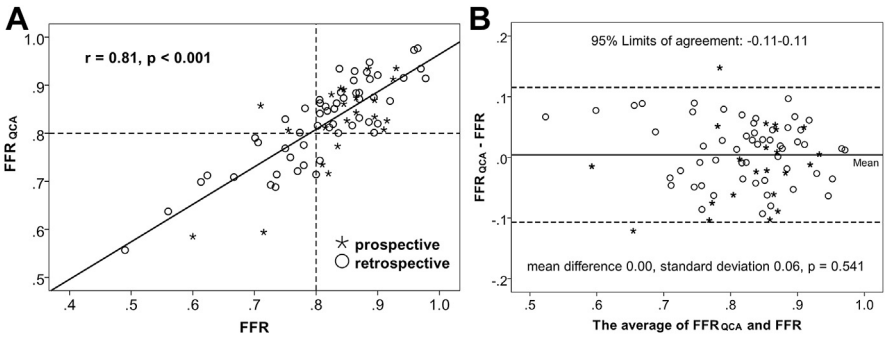

Figure 3. Correlation and Agreement Between FFR and the Computed FFR_{QCA}

A good correlation (r = 0.81) was observed **(A)**. Bland-Altman plot **(B)** shows good agreement. Abbreviations as in Figure 1.

additional time is required for 3D reconstruction and frame count evaluation, these steps can be greatly simplified when a seamless integrated workflow is implemented.

Computation of FFR_{QCA} on bifurcation lesions. Of note, it is important to accurately estimate flow distribution at the bifurcation. Because the resistances of the daughter branches are unknown, this information needs to be extracted from the imaging data. A highlighted novelty of the presented approach is the use of the reference vessel instead of the actual arterial lumen to determine the flow distribution. The rationale is that the hypothetical feeding territory of a branch is related to its lumen dimensions before narrowing (11), which can be approximated by the reference vessel in 3D QCA. This feeding territory will not change until collateral flow develops, which would be rather infrequent in the case of intermediate lesions. We applied bifurcation diameter models to generate more accurate reconstruction of the reference vessel in diffusely diseased branches. All of these attempts seemed to contribute to a simulation matching close to the actual coronary physiology.

Comparison to FFR_{CT}. Koo et al. (4) and Min et al. (5) reported a novel approach for the computation of FFR_{CT} from coronary computed tomography angiography data. Whereas FFR_{CT} and FFR_{QCA} both used CFD to solve Navier-Stokes equations, the fundamental difference was in the boundary conditions. Whereas FFR_{CT} estimated the total rest coronary flow relative to ventricular mass and assumed that microcirculation reacted predictably to the maximal hyperemic condition, FFR_{QCA} calculated hyperemic flow using 3D QCA and frame count directly on the angiographic projections during hyperemia. It appeared that FFR_{QCA} was more accurate than FFR_{CT}. This could be explained by the higher image resolution in x-ray angiography (≈0.2 mm) versus coronary computed tomography angiography (≈0.6 mm) (12), as well as by the presence of downstream microcirculatory disease (13). In this case,

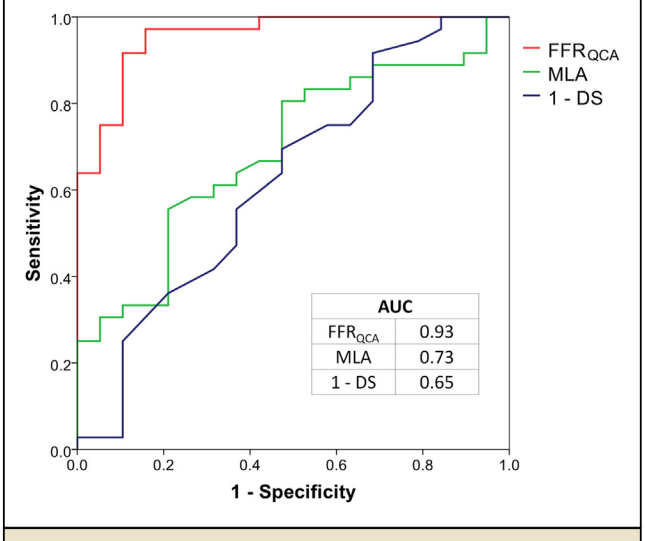

Figure 4. ROC Curves for the Discrimination of Functionally Significant Stenoses

Areas under the curve (AUC) for receiver-operating characteristics (ROC) for the prediction of FFR ≤0.80 by FFR_{QCA} and 3D QCA. MLA = minimum lumen area; DS% = percent diameter stenosis; other abbreviations as in Figure 1.

Table 3. Diagnostic Performance of FFR_{QCA} and 3D QCA Anatomical Indices

	FFR_{QCA} ≤0.80	MLA ≤2.11 mm^2	DS ≥50%
Accuracy	88 (81–96)	64 (53–75)	68 (57–78)
Sensitivity	78 (60–97)	83 (66–99)	52 (30–74)
Specificity	93 (85–100)	56 (42–69)	74 (62–86)
PPV	82 (64–99)	44 (29–60)	46 (26–67)
NPV	91 (83–99)	88 (77–100)	78 (67–90)

Values are n (95% CI).

3d = 3-dimensional; CI = confidence interval; DS = diameter stenosis; FFR = fractional flow reserve; FFR_{QCA} = computed fractional flow reserve by quantitative coronary angiography; MLA = minimum lumen area; NPV = negative predictive value; PPV = positive predictive value; QCA = quantitative coronary angiography.

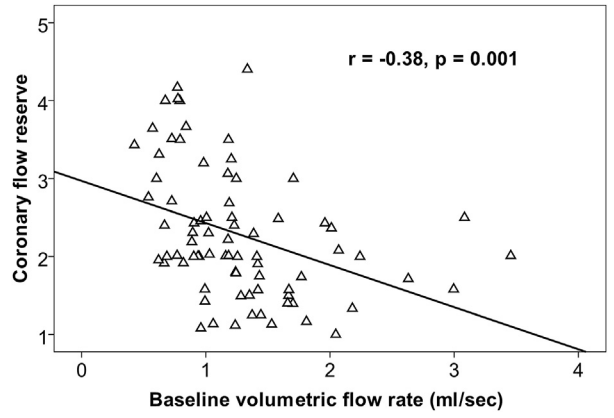

Figure 5. CFR and Baseline Volumetric Flow Rate

Wide scatter was observed, especially in vessels with low baseline volumetric flow. CFR = coronary flow reserve.

FFR_{CT} may be prone to more discrepancies with the measured FFR, whereas FFR_{QCA} can compensate these "confounders" by the hyperemic flow component. Because the hyperemic flow through a stenosis supplying such diseased territory will be lower, FFR_{QCA} will be higher. In addition, extracting accurate anatomical data by FFR_{CT} is more challenging in patients with advanced and calcified coronary artery disease and irregular heart rhythm, whereas in vivo lumen sizing by 3D QCA was demonstrated to have good agreement with intracoronary imaging (9). The shorter computational time is also an advantage of FFR_{QCA}.

Comparison to FFR. Morris et al. (7) presented a model to compute virtual FFR from rotational angiography. Generic microvascular resistance and compliance for the distal myocardial bed were assumed, which holds on average but will not apply to every individual patient (12). Our data showed a large spread in CFR around the group average, especially for patients with low baseline VFR, indicating that the increase in coronary flow as responded to hyperemia varies with wide scatter in individual patients. It was also admitted by the authors that virtual FFR applied a "one-size-fits-all" approach. As a result, the computed FFR was more likely to deviate from wire-based FFR in cases with abnormally microcirculatory resistance or downstream collateral circulation (12). On the contrary, FFR_{QCA} incorporates individual hyperemic flow, likely resulting in more realistic prediction of physiological behavior at the level of a single patient. The substantial gain in computational time and the ability of processing monoplane or biplane angiographic acquisitions are also advantages of FFR_{QCA}.

Table 4. Correlations Between FFR and Anatomical Indices

	Spearman Rho	p Value
Percent diameter stenosis	−0.26	0.025
Percent area stenosis	−0.27	0.019
Minimum lumen diameter	0.33	0.003
Minimum lumen area	0.40	0.000
Intraluminal plaque volume	−0.18	0.112

Potential clinical value and future of FFR_{QCA}. Although measurement of FFR is a safe procedure to perform, there is a small risk of injuring vessels by pressure wire manipulation. In a Nordic-Baltic bifurcation substudy, FFR measurements could not be obtained in 10% of the population due to side branch dissection by pressure wires and wiring failure (14). In addition, the use of pressure wires significantly increases the operational cost of diagnostic angiography. Development of algorithms that compute FFR from the angiographic data alone can increase the utility of FFR assessment.

FFR_{QCA}, empowered by reliable quantification of vessel dimensions, offers a novel and accurate tool for the fast computation of FFR plus anatomical details that can be used for assessing optimal angiographic projections and optimal stent sizing if subsequent revascularization is planned. The reconstruction of virtual FFR pullback by FFR_{QCA} could identify precise targets for further intervention on the basis of focal, rather than diffuse pressure loss.

At present, the computation of FFR_{QCA} requires quite some user interactions. Substantial automation should be implemented to enable high volume use. Different cardiac phases are associated with different flow profiles, resulting in variability in the estimation of flow transport time by frame count. We used mean VFR, which integrated contrast transport time and lumen volume by coronary tree reconstruction, to minimize the variability of FFR_{QCA}. This potentially contributed to more reliable estimation of VFR compared with reconstruction of a single coronary vessel neglecting the flow in the side branches. Nevertheless, timing of contrast injection can still influence the result. Therefore, the use of an electrocardiogram-triggered or wave-free–modulated injector might further improve FFR_{QCA}, though routine diagnostic angiography is often performed with manual injections and it has been shown that injection rate had only minor impact on TIMI frame count (15) and CFR on the basis of hyperemic frame count data had a strong correlation with the Doppler-wire derived CFR (16). In another study, hyperemic frame count data were used to calculate FFR using flow equations on simple lesions (17). Good correlation between the calculated and the measured values was found.

Despite that angiographic frame rate and administration route of vasodilators were found to have minor impact on the deviation of FFR_{QCA}, it should be stressed that the population size was too limited to draw final conclusions about the sensitivity and specificity of this novel

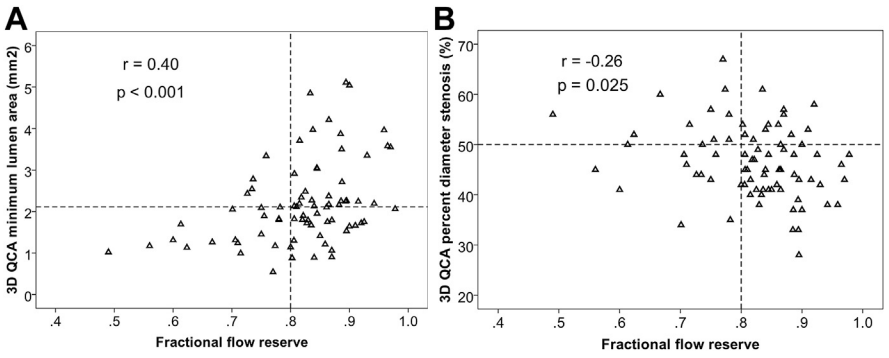

Figure 6. Correlation Between FFR and Anatomical Indices

A moderate correlation (r = 0.40) between FFR and minimum lumen area **(A)** and a weak correlation (r = −0.26) between FFR and percent diameter stenosis **(B)** were observed. Abbreviations as in Figure 1.

computational method. Further studies to test the impact of these variants on FFR_{QCA} using controlled and optimized processes are required. A multicenter and larger study will be necessary to further validate FFR_{QCA}. Finally, the 10-min processing time, including manual interaction, must be shortened for this technique to be accepted in routine clinical use.

Study limitations. The study was limited by its small sample size. We only validated FFR_{QCA} on de novo lesions. Selection bias might be involved. The fusion of x-ray angiography with intravascular imaging (18) might provide more accurate anatomical models. However, this setting is more technically demanding and intravascular imaging itself is not devoid of artifacts.

The angiographic reconstruction and frame count estimation were performed by an experienced analyst in a core laboratory and, hence, the accuracy of FFR_{QCA} operated in a fully integrated workflow needs to be verified when applied by the medical and technical staff.

Table 5. Reproducibility in Modeling FFR_{QCA}

	Intraobserver Variability	Interobserver Variability
Minimum lumen diameter, mm	0.02 ± 0.08	0.03 ± 0.11
Minimum lumen area, mm^2	0.02 ± 0.21	0.04 ± 0.40
Reference vessel diameter, mm	0.00 ± 0.12	0.12 ± 0.16
Percent diameter stenosis	0.30 ± 2.00	0.50 ± 4.09
Percent area stenosis	1.21 ± 3.82	1.52 ± 5.60
Intraluminal plaque volume, mm^3	7.92 ± 24.88	9.53 ± 20.04
Lesion eccentricity index	0.04 ± 0.10	0.05 ± 0.09
Mean flow rate, ml/s*	0.12 ± 0.17	0.37 ± 0.42
FFR_{QCA}	0.00 ± 0.03	0.01 ± 0.03

Values are mean ± SD. *Reported for the mother vessel if bifurcation models were applied.
FFR_{QCA} = computed fractional flow reserve by quantitative coronary angiography.

Among consecutive patients, we included only those with FFR measurements and hyperemic projections recorded by flat-panel systems, implying that the diagnostic performance of FFR_{QCA} needs to be verified in an all-comers population undergoing diagnostic angiography. Nevertheless, the current results obtained in a rather challenging patient subset with moderate stenosis are very encouraging and warrant a larger study.

Conclusions

Computation of FFR_{QCA} is a novel method that allows the assessment of the functional significance of intermediate stenosis. It may emerge as a safe, efficient, and cost-reducing tool for evaluation of coronary stenosis severity during diagnostic angiography.

Acknowledgment
The authors thank Dr. Stylianos A. Pyxaras for his contribution to the data collection.

Reprint request and correspondence: Dr. Shengxian Tu, Division of Image Processing, Department of Radiology, Leiden University Medical Center, Albinusdreef 2, 2333 ZA, Leiden, the Netherlands. E-mail: S.T.Tu@lumc.nl.

REFERENCES

1. De Bruyne B, Pijls NH, Kalesan B, et al., for the FAME 2 Trial Investigators. Fractional flow reserve-guided PCI versus medical therapy in stable coronary disease. N Engl J Med 2012;367:991–1001.
2. Tonino PA, De Bruyne B, Pijls NH, et al., for the FAME Study Investigators. Fractional flow reserve versus angiography for guiding percutaneous coronary intervention. N Engl J Med 2009;360:213–24.
3. Kern MJ, Samady H. Current concepts of integrated coronary physiology in the catheterization laboratory. J Am Coll Cardiol 2010;55:173–85.

4. Koo BK, Erglis A, Doh JH, et al. Diagnosis of ischemia-causing coronary stenoses by noninvasive fractional flow reserve computed from coronary computed tomographic angiograms: results from the prospective multicenter DISCOVER-FLOW (Diagnosis of Ischemia-Causing Stenoses Obtained Via Noninvasive Fractional Flow Reserve) study. J Am Coll Cardiol 2011;58:1989–97.
5. Min JK, Leipsic J, Pencina MJ, et al. Diagnostic accuracy of fractional flow reserve from anatomic CT angiography. JAMA 2012;308:1237–45.
6. Wijns W. The one-stop shop offering both coronary anatomy and myocardial perfusion: may well be opening soon, around the corner. J Am Coll Cardiol Img 2012;5:1112–4.
7. Morris PD, Ryan D, Morton AC, et al. Virtual fractional flow reserve from coronary angiography: modeling the significance of coronary lesions: results from the VIRTU-1 (VIRTUal Fractional Flow Reserve From Coronary Angiography) study. J Am Coll Cardiol Intv 2013;6:149–57.
8. Wijns W, Kolh P, Danchin N, et al., for the Task Force on Myocardial Revascularization of the ESC, EACTS, EAPCI. Guidelines on myocardial revascularization. Eur Heart J 2010;31:2501–55.
9. Tu S, Xu L, Ligthart J, et al. In vivo comparison of arterial lumen dimensions assessed by co-registered three-dimensional (3D) quantitative coronary angiography, intravascular ultrasound and optical coherence tomography. Int J Cardiovasc Imaging 2012;28:1315–27.
10. Huo Y, Finet G, Lefèvre T, Louvard Y, Moussa I, Kassab GS. Optimal diameter of diseased bifurcation segment: a practical rule for percutaneous coronary intervention. EuroIntervention 2012;7:1310–6.
11. West GB, Brown JH, Enquist BJ. A general model for the origin of allometric scaling laws in biology. Science 1997;276:122–6.
12. Johnson NP, Kirkeeide RL, Gould KL. Coronary anatomy to predict physiology: fundamental limits. Circ Cardiovasc Imaging 2013;6:817–32.
13. De Bruyne B, Bartunek J, Sys SU, Heyndrickx GR. Relation between myocardial fractional flow reserve calculated from coronary pressure measurements and exercise-induced myocardial ischemia. Circulation 1995;92:39–46.
14. Kumsars I, Narbute I, Thuesen L, et al., for the Nordic-Baltic PCI Study Group. Side branch fractional flow reserve measurements after main vessel stenting: a Nordic-Baltic Bifurcation Study III substudy. EuroIntervention 2012;7:1155–61.
15. Dodge JT Jr, Rizzo M, Nykiel M, et al. Impact of injection rate on the Thrombolysis In Myocardial Infarction (TIMI) trial frame count. Am J Cardiol 1998;81:1268–70.
16. Stoel MG, Zijlstra F, Visser CA. Frame count reserve. Circulation 2003;107:3034–9.
17. Kőszegi Z, Tar B. Prediction of fractional flow reserve using contrast media flow data under vasodilatation and the parameters of 3D coronary angiography (abstr.). J Am Coll Cardiol 2012;60:B67–8.
18. Tu S, Pyxaras SA, Li Y, Barbato E, Reiber JH, Wijns W. In vivo flow simulation at coronary bifurcation reconstructed by fusion of 3-dimensional x-ray angiography and optical coherence tomography. Circ Cardiovasc Interv 2013;6:e15–7.

Key Words: cardiovascular physiology ■ computational fluid dynamics ■ fractional flow reserve ■ quantitative coronary angiography.